Front. Environ. Sci. Eng. 2021, 15(5): 101
https://doi.org/10.1007/s11783-021-1388-4

RESEARCH ARTICLE

Effects of different types of biochar on the properties and reactivity of nano zero-valent iron in soil remediation

Chengjie Xue [1#], Juan Wu [2#], Kuang Wang[1,3], Yunqiang Yi (✉)[1,3,4], Zhanqiang Fang (✉)[1,3,4], Wen Cheng[1], Jianzhang Fang[1,3,4]

1 School of Environment, South China Normal University, Guangzhou 510006, China
2 Institute of Environmental Sciences (CML), Leiden University, Leiden 2300 RA, The Netherlands
3 Guangdong Technology Research Center for Ecological Management and Remediation of Water System, Guangzhou 510006, China
4 Guangdong Provincial Key Laboratory of Chemical Pollution & Environmental Safety, Guangzhou 510006, China

HIGHLIGHTS

- Biochar enhanced the mobility and stability of zero-valent iron nanoparticles.
- Particle performance was best when the BC:nZVI mass ratio was 1:1.
- Bagasse-BC@nZVI removed 66.8% of BDE209.

ARTICLE INFO

Article history:
Received 14 July 2020
Revised 7 December 2020
Accepted 8 December 2020
Available online 27 February 2021

Keywords:
Nano zero-valent iron
Biochar
BDE209
Transport
Soil

GRAPHIC ABSTRACT

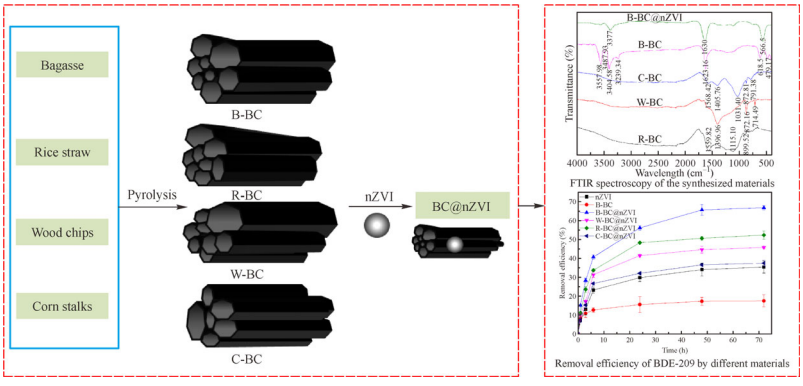

ABSTRACT

The addition of nano zero-valent iron (nZVI) is a promising technology for the in situ remediation of soil. Unfortunately, the mobility and, consequently, the reactivity of nZVI particles in contaminated areas decrease due to their rapid aggregation. In this study, we determined how nZVI particles can be stabilized using different types of biochar (BC) as a support (BC@nZVI). In addition, we investigated the transport behavior of the synthesized BC@nZVI particles in a column filled with porous media and their effectiveness in the removal of BDE209 (decabromodiphenyl ether) from soil. The characterization results of N_2 Brunauer–Emmett–Teller (BET) surface area analyses, scanning electron microscopy (SEM), X-ray diffraction (XRD) and Fourier transform infrared spectroscopy (FTIR) indicated that nZVI was successfully loaded into the BC. The sedimentation test results and the experimental breakthrough curves indicated that all of the BC@nZVI composites manifested better stability and mobility than did the bare-nZVI particles, and the transport capacity of the particles increased with increasing flow velocity and porous medium size. Furthermore, the maximum concentrations of the column effluent for bagasse–BC@nZVI (B–BC@nZVI) were 19%, 37% and 48% higher than those for rice straw–BC@nZVI (R–BC@nZVI), wood chips–BC@nZVI (W–BC@nZVI) and corn stalks–BC@nZVI (C–BC@nZVI), respectively. A similar order was found for the removal and debromination efficiency of decabromodiphenyl ether (BDE209) by the aforementioned particles. Overall, the attachment of nZVI particles to BC significantly increased the reactivity, stability and mobility of B–BC@nZVI yielded, and nZVI the best performance.

1 Introduction

Products containing BDE209, a homolog of polybrominated diphenyl ethers (PBDEs), have been used in numerous industries due to the good flame retardant performance of the substance (La Guardia et al., 2006;

✉ Corresponding authors
E-mail: 20200582@m.scnu.edu.cn (Y. Yi); zhanqiangfang@m.scnu.edu.cn (Z. Fang)

[#]Both authors contributed equally to this work and share first authorship

Cincinelli et al., 2012; Abbasi et al., 2019). However, when PBDEs enter the environment, their strong hydrophobicity and persistence lead to their retention in soil or sediment rather than in water (Chokwe et al., 2019). PBDEs are highly toxic, persistent and bioaccumulative and can cause certain harm to the ecological environment, animals and human body (Xie et al., 2014). PBDEs have toxic and carcinogenic effects on the brain, liver, kidney, endocrine system, reproductive development system and nervous system (Meerts et al., 2001). PBDEs can cause an imbalance in thyroid hormones, affect metabolic function, make movement behavior abnormal and learning ability decline (Eriksson et al., 2001). PBDEs severely contaminate soils and sediments, possibly posing a serious threat to human health and environmental safety (Hites, 2004; Zhang et al., 2015). Therefore, it is necessary to develop effective and inexpensive technologies to remediate soils contaminated with PBDEs. Currently, information about the remediation of BDE209-contaminated soil using different types of biochar (BC) loaded with nano zero-valent iron (nZVI) is limited.

Laboratory studies have shown that nZVI is an effective reductant for removing PBDEs from aqueous or organic phases due to its large contact area with pollutants and strong reducibility (Lowry and Johnson, 2004; Keum and Li, 2005; Fang et al., 2011). For example, Shih and Tai reported that nZVI degraded more than 90% of BDE209 in an aqueous solution in 40 min (Shih and Tai, 2010), and the degradation efficiency was considerably higher than that of ZVI. Fang et al. demonstrated that 98% of BDE209 (2 mg/L) was removed within 24 h by nZVI (4 g/L) (Fang et al., 2011), which was higher than the removal rate achieved with bare-ZVI. Recently, the direct injection of nZVI into groundwater or soil contaminated with pollutants has attracted considerable attention from researchers (Quinn et al., 2005; Baumann, 2010; He et al., 2010). However, to realize such applications, some existing technical problems must be solved. First, the surface of bare-nZVI is easily oxidised, leading to the formation of a protective layer on the surface of the particles. This reduces the effective contact area between contaminants and nZVI particles, which is not conducive to pollutant removal. Second, due to van der Waals forces and magnetic attraction, nZVI particles tend to aggregate rapidly, which decreases their reduction capacity. Third, the transfer of agglomerated particles in the soil matrix is poor, which means that they will probably not be transported to the target contaminated area (Chekli et al., 2016). Previous investigations have demonstrated that the transportation of non-stabilized or aggregated ZVI nanoparticles in soil is limited and difficult (He et al., 2007; Kanel et al., 2008). Therefore, the key problems that must be solved to facilitate the effective and widespread use of nZVI in contaminated soils are overcoming the instability and improving the transportability of nZVI in soils.

BC is an excellent environmentally friendly and cost-controllable environmental remediation agent because it is producted by the pyrolysis of waste plant biomass in an inert gas atmosphere. Moreover, BC can be used to remove various pollutants and improve soil fertility (Bolan et al., 2014; Mohamed et al., 2017; Wang et al., 2019). To address the key problems mentioned in the preceding paragraph, one approach is to use BC as a support to disperse particles and decrease particle agglomeration. BC seems to be suitable for this purpose because of its stable structure, high porosity, large specific surface area (SSA) and abundant surface functional groups (Zhou et al., 2014). For instance, Yan et al. found that nZVI did not agglomerate on the surface of BC and dispersed uniformly (Yan et al., 2015). Su et al. indicated that the stability and fluidity of BC particles loaded with nZVI particles and their removal rate of hexavalent chromium were considerably higher than those of bare-nZVI particles (Su et al., 2016). However, research on the degradation of PBDEs in soil by using BC loaded with nZVI particles is rare. Moreover, the physicochemical and structural properties of BC, such as SSA, surface functional groups and particle size, are affected by the pyrolysis temperature and source of BC (Yi et al., 2019). Wang et al. showed that the fluidity of BC is higher when the pyrolysis temperature is lower and the BC particle diameter is smaller (Wang et al., 2013a). Thus, the transport and reactivity of BC-supported nZVI composites (BC@nZVI) might also be controlled by the pyrolysis temperature and feedstock source of the BC. However, it is unclear whether the BC feedstock species affects BC@nZVI transport and reactivity in the removal of BDE209 from soil.

Therefore, the purposes of this study are to 1) synthesize stabilized nZVI particles supported on different types of BC, characterize them and compare their stability with that of bare-nZVI; 2) explore the effects of multiple factors on the fluidity of BC@nZVI in column experiments, including BC species, BC pyrolysis temperature, and BC:nZVI mass ratio; and 3) compare the removal and debromination efficiencies of BDE209 obtained in multiple related contact experiments of BC, nZVI nanoparticles and BC@nZVI particles.

2 Materials and methods

2.1 Test soil

The test soil used in this experiment was collected from the Higher Education Mega Center (China), and the several properties of the soil are listed in Table S1 (Appendix material). The soil, processed as described above, was artificially contaminated using our previously reported method (Wu et al., 2016).

2.2 Synthesis and characterization of particles

All of the reagents used in this experiment are listed in Appendix A1 (Appendix material). The nZVI particles were prepared by following the method reported previously by our team (Fang et al., 2011). BCs were derived from the pyrolysis of bagasse (B-BC), wood chips (W-BC), corn stalks (C-BC) or rice straw (R-BC) at 600°C for 2 h in a muffle furnace under constant purging with nitrogen gas, and the resulting products were ground. BC@nZVI samples were synthesized by following the $NaBH_4$ reduction method. The steps of the synthesis method are given in Supplementary Appendix A1.

The N_2 Brunauer–Emmett–Teller (BET) surface area analysis, surface zeta potential and hydrodynamic diameter analysis, scanning electron microscopy (SEM), Fourier transform-infrared (FTIR) spectrometric analysis and X-ray diffraction analysis are detailed in Supplementary Appendix A1.

2.3 Sedimentation tests

By measuring the sedimentation rate of the particle suspensions, the stability values of the various types of BC@nZVI suspensions were compared with the stability of bare-nZVI. The concentrations of the different types of BC@nZVIs and bare-nZVI in the suspensions (with consistent iron content) were monitored continuously at 508 nm by using an ultraviolet (UV, L5S Inesa analytical instrument Co. Ltd, China)-visible spectrophotometer after subjecting them to ultrasonic treatment for 5 min.

2.4 Column experiments

Transport studies were performed in silica-sand-packed vertical glass columns (1.5 cm i.d., 12 cm length). Prior to being used in the experiments, the sand was sequentially soaked in 0.1 mol/L sodium dithionite and hydrogen peroxide (5%) for 2 h to remove metal oxides and other substances on the surface. Thereafter, the sand was soaked in hydrochloric acid (12 mol/L) solution overnight, washed thrice with deionised water and dried. The following operations were performed as reported by Liang et al. (Liang et al., 2014), with a slight modification. A nylon screen (80 mesh) was installed at the bottom of the column, which was then filled with silica sand. Detailed experimental details are given in Supplementary Appendix A2. The specific formula of debromination efficiency is as follows Eq. (1) in Supplementary Appendix A2.

2.5 Experimental set-up

Sacrificial experiments were carried out in ambient air. Detailed experimental details are given in Supplementary Appendix A2.

The BDE209 concentrations in the extracts were quantified using a Shimadzu high-performance liquid chromatograph (HPLC, HP1100, Japan). Detailed experimental details are given in Supplementary Appendix A2.

The Br^- concentration was determined using an ion chromatograph (IC, ICS-900, USA). Detailed experimental details are given in Supplementary Appendix A2.

3 Results and discussion

3.1 Characterization of particles

The SSA, elemental composition and physicochemical properties of the four types of BC synthesized herein are summarized in Table S2. All four types of BCs were alkaline, with only slightly differing pH values, which is conducive to regulating the pH of acidic soils (Chintala et al., 2014). Moreover, the organic matter and S contents in the four BCs decreased in the following order: B-BC>R-BC>W-BC>C-BC. Furthermore, the C/H ratio was the highest in B-BC, followed by C-BC, W-BC and R-BC. This means that B-BC had the highest degree of aromatisation (i.e., a more perfect π-conjugated aromatic structure (Keiluweit et al., 2010)), and the stabilization of nZVI by BC was the highest in the case of B-BC. According to the BET results, the SSAs of B-BC, W-BC, C-BC and R-BC were 352.6, 42.1, 39.0 and 171.5 m^2/g, respectively. The total pore volume (PV) and SSA of B-BC and R-BC were considerably higher than those of the other BCs, which is beneficial for nZVI loading. In addition, the BET-determined SSAs of B-BC@nZVI (BC:nZVI mass ratio of 1:1) and bare-nZVI were 71 and 35 m^2/g, respectively. The BET-determined SSA of B-BC@nZVI was considerably smaller than that of B-BC, which indicated that nZVI was effectively loaded into the BC and that the BC pores may have been blocked by the loaded nZVI (Zhuang et al., 2011).

SEM analyses were performed to observe the morphologies of B-BC, nZVI and B-BC@nZVI (Figs. 1(a)–1(c)). The SEM surface morphology clearly revealed that the BC particles had an abundant porous structure, which provided appropriate sites to support nZVI. The bare-nZVI particles aggregated to form chain structures or clusters due to the strong agglomeration effect. In contrast, the nZVI particles in BC@nZVI (BC:nZVI = 1:1) were observed to be well scattered throughout the porous structure and on the surface of the BC, which prevented their aggregation to some extent. The X-ray diffraction patterns of the BCs and the synthesized composites are shown in Figs. 1(d) and 1(e). All of the BCs had similar diffractogram patterns, except for a few minor differences in the shape and strength of the peaks, thus indicating that the amorphous materials had poor crystallinity and carbon-rich phases. A few sharp peaks were observed in the spectrum of BC,

indicating the presence of inorganic components, such as SiO_2 ($2\theta = 28°$), KCl ($2\theta = 39.5°$) (Ahmad et al., 2018) and $CaCO_3$ (peak at 2θ = 29.2°, present only in C-BC), as confirmed in previous studies (Wu et al., 2012; Devi and Saroha, 2014). For BC loaded with nZVI, a significant peak at 2θ = 44.9° was observed for all four types of BC@nZVI, thus confirming the presence of ZVI (α-Fe^0) in all of the composites. The results further revealed that the nZVI particles were successfully loaded onto the BCs. To identify the surface properties of the samples, FTIR spectra of different BCs and B-BC@nZVI were generated within 400–4000 cm^{-1} (Fig. 1(f)). The results suggested that the BCs were rich in organic functional groups. Moreover, the intense adsorption band at 566.5 cm^{-1} in the B-BC@nZVI spectrum shown in Fig. 1(f) indicated that Fe–O bonds were formed between BC and nZVI (Liu et al., 2010; Cazetta et al., 2016). Vibrations of aromatic –CH groups were observed for R-BC, W-BC and C-BC at wavenumbers of 714.49–899.52 cm^{-1}, indicating the presence of adjacent aromatic hydrogen (Ahmad et al., 2012). The signals at 1115.1 cm^{-1} and 1031.4 cm^{-1} for R-BC and C-BC, respectively, were assigned to C–O functional groups. The peaks near 1400 cm^{-1} represented aromatic ring modes, which were present in the W-BC and C-BC samples. The peaks at approximately 1560 cm^{-1} (R-BC and C-BC) and 1620 cm^{-1} (B-BC and B-BC@nZVI) corresponded to C = C and C = O stretching vibrations, respectively. Notably, clear bands at approximately 3200–3550 cm^{-1} appeared only in the spectrum of B-BC. These bands are associated with-OH stretching and hydroxyl functional group stretching vibrations, indicating the presence of hydroxyl groups on the surface of the B-BC samples (Wang et al., 2013b). In sum, the results suggested that the synthesized BCs were rich in organic functional groups. However, there were a few significant differences between the FTIR (detailed results and discussions are given in Appendix A3) spectra of B-BC and B-BC@nZVI. For instance, considerably lower absorption intensities were observed at approximately 3400 cm^{-1} and 1630 cm^{-1} for B-BC@nZVI than B-BC, which can potentially be attributed to the reaction between nZVI and BC. The results described above were confirmed by the XRD patterns of the materials.

3.2 Stability assessment

The stability of nanoparticles in practical engineering applications is of great significance. The sedimentation curves of the four types of BC@nZVI composites synthesized herein are exhibited in Fig. 2(a). The experimental data indicated that the absorbance of nZVI at 508 nm decreased rapidly by 35% within 2 min, and the relative absorbance tended to be stable after 10 min at 29% of the initial value. After 10 min, the absorbance of R-BC@nZVI and W-BC@nZVI decreased by 31% and 20%, respectively, compared with their respective initial absor-

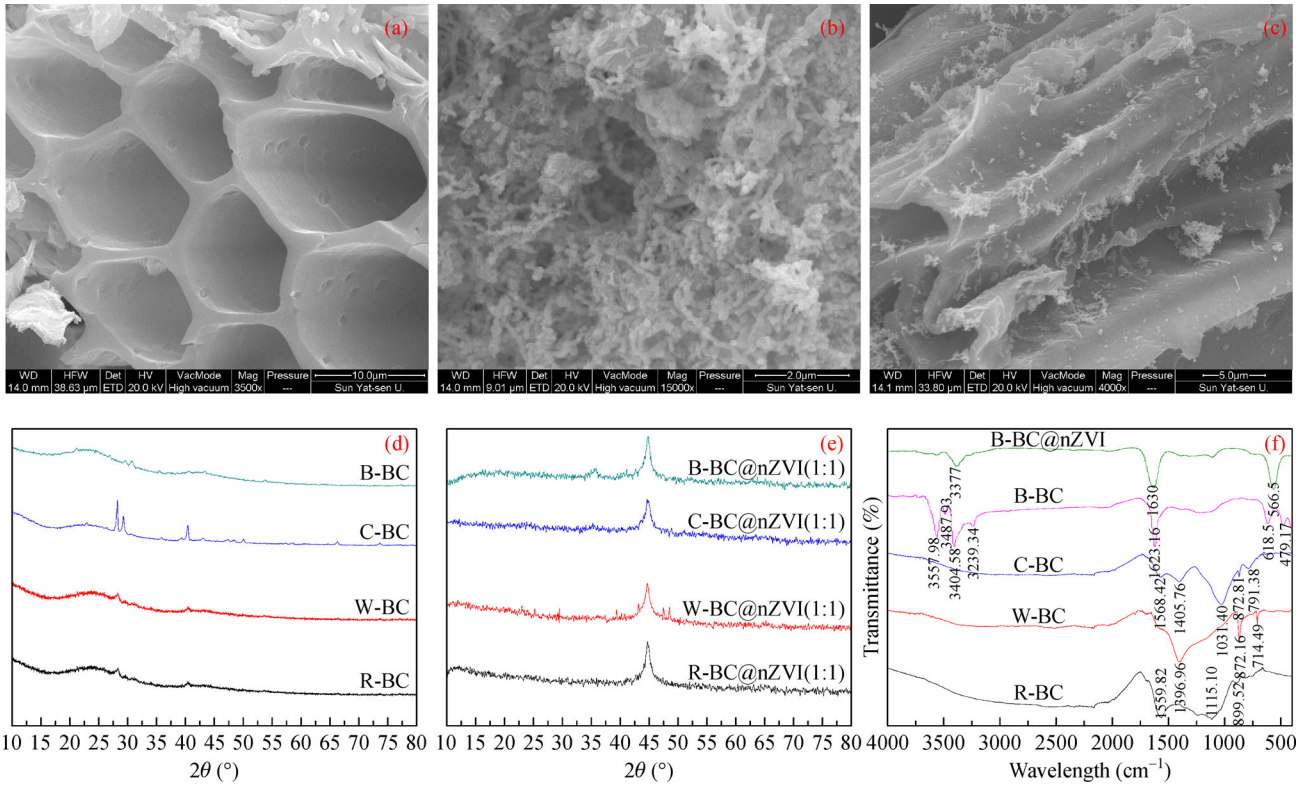

Fig. 1 SEM images of (a) B-BC, (b) nZVI and (c) B-BC@nZVI; (d, e) XRD patterns and (f) FTIR spectra of the synthesized materials.

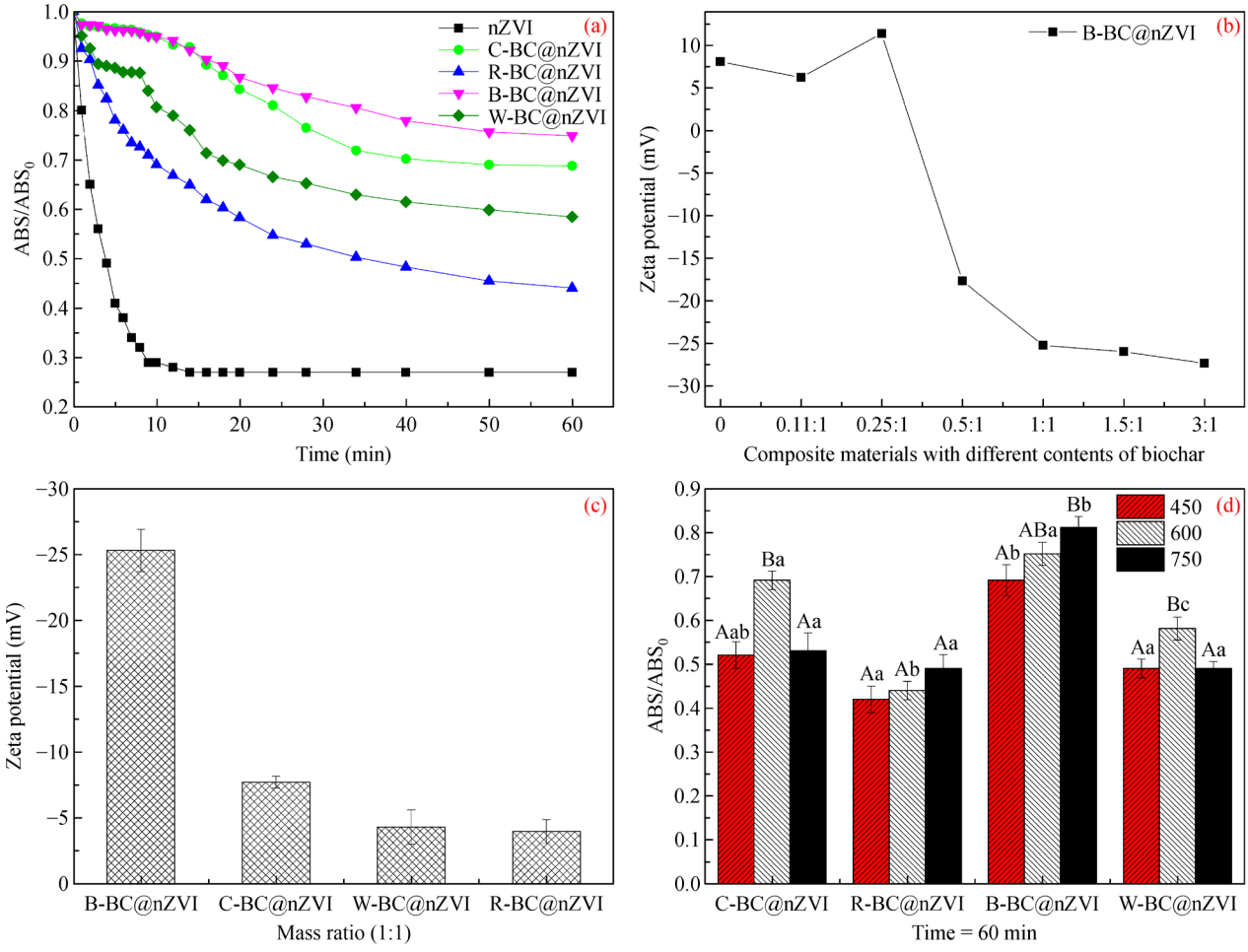

Fig. 2 (a) Sedimentation tests for different particles; (b) effects of BC/nZVI mass ratio on the zeta potential for BC@nZVI composites; (c) effects of biochar types on the zeta potential for BC@nZVI composites; (d) effects of biochar pyrolysis temperature on particles stability. The capital letters represent significant differences of same particles at different temperature while lowercase letters represent significant differences of different particles at the same temperature ($p < 0.05$).

bance values. The absorbance values of B-BC@nZVI and C-BC@nZVI remained stable for the first 10 min, after which they tended to decrease slowly to finally reach a stable state. After 60 min, the relative absorbance values of the B-BC@nZVI, C-BC@nZVI, W-BC@nZVI and R-BC@nZVI composites were 47.8%, 41.7%, 31.4% and 17.0% higher than the absorbance value of bare-nZVI. This result implied that all BC@nZVI composites were more stable than bare-nZVI. B-BC@nZVI exhibited the highest stability among the four composites. The large decrease in the absorbance of bare-nZVI was caused by its rapid deposition, which was ascribed to the effective aggregation of nZVI particles due to electrostatic attraction (Tiraferri et al., 2008). In the BC@nZVI composites, attachment of nZVI particles on the porous and rough surfaces of BC prevented agglomeration and enhanced the stability of the nZVI particles, as confirmed by SEM and the literature (He and Zhao, 2005; Xu et al., 2010). The order of stability of the four BC@nZVI composites was the same as the order of the C:H ratio in the BCs (Table S2). According to Keiluweit et al. (Keiluweit et al., 2010), the degree of aromatisation and stabilization of BCs increases with the C/H ratio; we believe that the C/H ratio is the main reason for the differences in the sedimentation test results for the four types of BC@nZVI composites in this study (Fig. 2). Among the BC@nZVI composites with different BC:nZVI mass ratios, the mass ratio of 1:1 gave the highest stability in all of the types of composites (Fig. 3). The stability of the composites increased when the BC content increased from 0.11:1 to 1:1. However, with subsequent increases in BC content, the stability of the composites decreased, possibly because the excess BC increased the particle size, thus facilitating the overall settling of BC@nZVI. Similar results were found in the removal of BDE209 from soil by using B-BC@nZVI composites with different BC:nZVI mass ratios (detailed results and discussions are given in Appendix A4 in the Supplementary material). Therefore, the BC@nZVI composite with a BC:nZVI mass ratio of 1:1 was used in subsequent experiments.

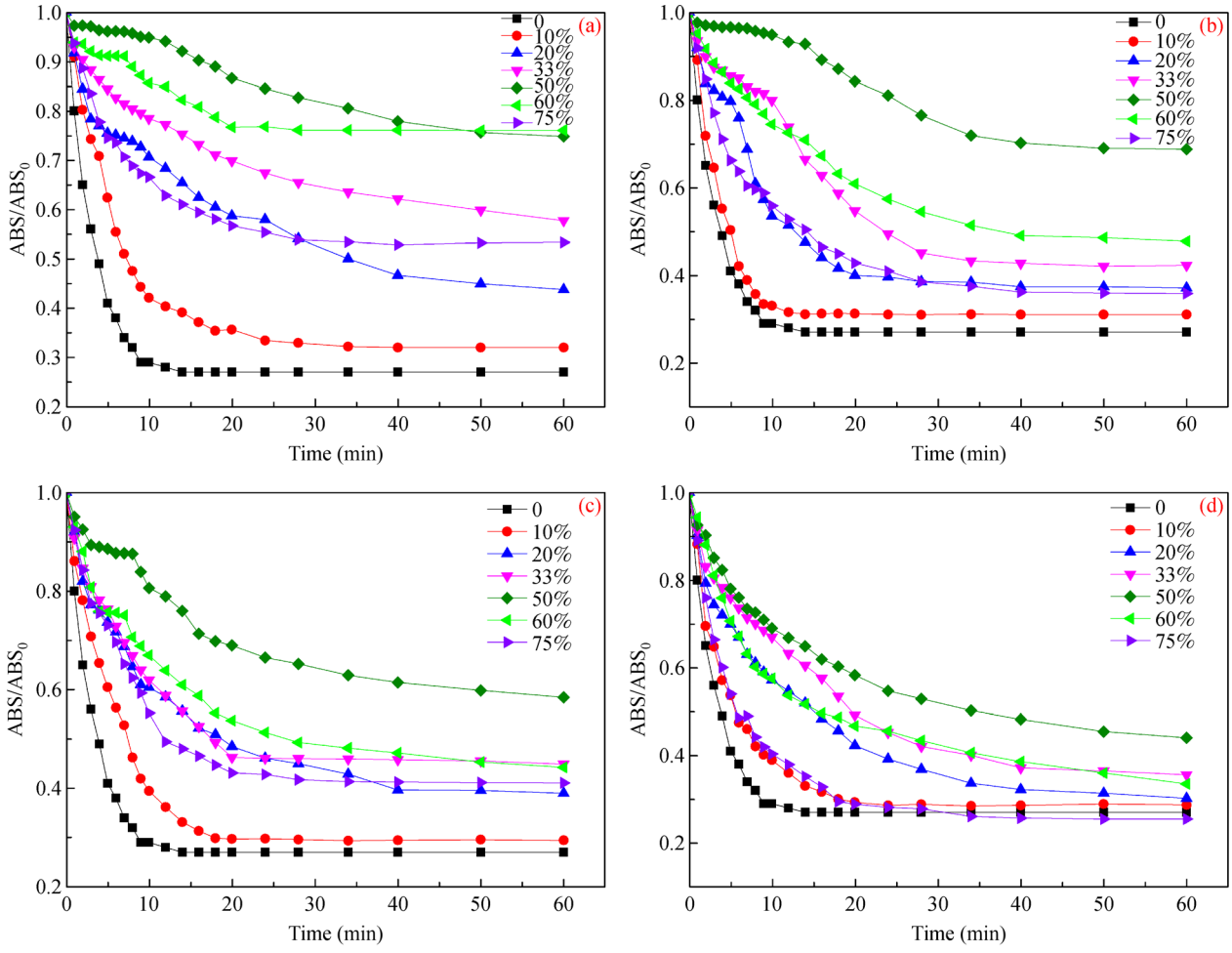

Fig. 3 Sedimentation tests of four BC@nZVI composites at different BC:nZVI mass ratios: (a) B-BC@nZVI, (b) C-BC@nZVI, (c) W-BC@nZVI, and (d) R-BC@nZVI.

The zeta potentials of the materials were also determined to assess their stability. The effects of different B-BC:nZVI mass ratios on the stability of the B-BC@nZVI composites, as measured using the zeta potentials, are illustrated in Fig. 2(b). The zeta potential was measured with Watson's distilled water at pH = 5.16. The experimental data demonstrated that the stability of B-BC@nZVI (1:1) (–25.25 mV) was approximately 3.14, 4.08, 2.23 and 1.43 times higher than that of B-BC@nZVI at mass ratios of 0:1, 0.11:1, 0.25:1 and 0.5:1, respectively. Notably, the zeta potentials of bare-nZVI, B-BC@nZVI (0.11:1) and B-BC@nZVI (0.25:1) were positive, whereas the zeta potential of B-BC@nZVI (0.5:1) was negative. This result occurred because nZVI particles are positively charged, whereas B-BC is negatively charged. It can be deduced from Fig. 2(c) that the absolute value of the zeta potential decreased in the following order: B-BC@nZVI>C-BC@nZVI>W-BC@nZVI>R-BC@nZVI>nZVI. Thus, based on the above results, it can be concluded that the use of BC as a support to synthesize BC@nZVI successfully improved the stability of nZVI.

The stability of BC-supported nZVI obtained at different pyrolysis temperatures was also studied. As illustrated in Fig. S1, the stability of the B-BC@nZVI composite increased as the pyrolysis temperature increased. According to the literature (Cantrell et al., 2012; Wang et al., 2013a), higher pyrolysis temperatures lead to a higher SSA of BC, which is better for reducing the aggregation of nZVI. However, different change trends in the absorbances of C-BC@nZVI and W-BC@nZVI with pyrolysis temperature were observed in this study (Figs. 2(d) and S1). After 60 min of sedimentation (Fig. 2(d)), the stability values of the C-BC@nZVI and W-BC@nZVI composites synthesized at 600°C were the highest, but there were no significant differences between the C-BC@nZVI and W-BC@nZVI composites synthesized at 450°C and those synthesized at 700°C. Similar results were found for the B-BC@nZVI and R-BC@nZVI composites, and the stability values of the materials synthesized at 600°C were not significantly different from those of the materials synthesized at 450°C or 700°C. Therefore, a pyrolysis temperature of 600°C was selected to produce BC for use in subsequent experiments.

Among the BC@nZVI composites with different BC:nZVI mass ratios, the mass ratio of 1:1 gave the highest stability in all of the types of composites (Fig. 3). The

stability of the composites increased when the BC content increased from 0.11:1 to 1:1. However, with subsequent increases in BC content, the stability of the composites decreased, possibly because the excess BC increased the particle size, thus facilitating the overall settling of BC@nZVI. Similar results were found in the removal of BDE209 from soil by using B-BC@nZVI composites with different BC:nZVI mass ratios (detailed results and discussions are given in Appendix A4 in the Supplementary material). Therefore, the BC@nZVI composite with a BC:nZVI mass ratio of 1:1 was used in subsequent experiments.

3.3 Column experiments

3.3.1 Effect of flow velocity on BC@nZVI transport

The effects of the BC:nZVI mass ratio and the pyrolysis temperature on BC@nZVI transport were studied by conducting a series of column tests. The results (shown in Figs. 4 and S2) were consistent with the stability results, which confirmed that the best mobility of the BC@nZVI composites was observed when the BC:nZVI mass ratio was 1:1 and the pyrolysis temperature was 600°C.

The injected flow velocity and the size of the soil particles were the key factors determining nanoparticle transport in the soil. The transportation results for the B-BC@nZVI composites in the silica sand column with variable flow velocity are shown in Fig. 5(a). The flow velocity significantly influenced the transport of the particles through the silica sand column because the particle mobility increased as the flow velocity increased. For instance, the maximum breakthrough C/C_0 increased from 0.58 to 0.74 as the flow velocity increased from 0.05 to 0.11 mL/s. Moreover, the highest effluent concentration at the flow rate of 0.15 mL/s was 0.85, which was 27% and 11% higher than those at flow rates of 0.05 and 0.11 mL/s, respectively. This may have occurred because of the increase in shearing forces with the increase in the flow

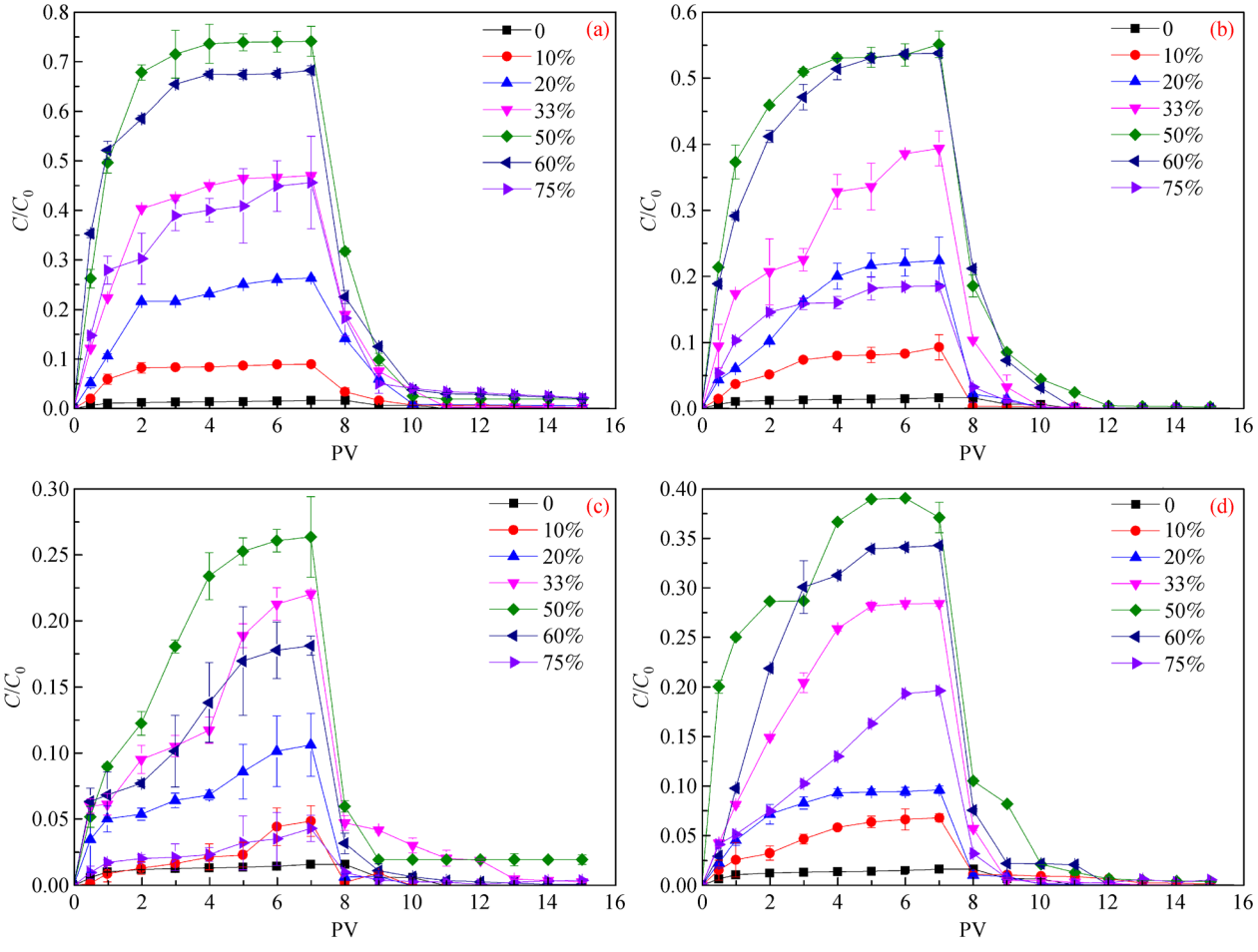

Fig. 4 Breakthrough curves of four BC@nZVI composites at different BC:nZVI mass ratios: (a) B-BC@nZVI, (b) R-BC@nZVI, (c) C-BC@nZVI, and (d) W-BC@nZVI.

velocity, which consequently enhanced the effluent concentration. The smaller viscous volume and higher resistance of the stable nZVI particles were also considered to contribute to their enhanced mobility because these factors enhance elution (Wang et al., 2013a; Zhang et al., 2017).

3.3.2 Effect of porous media on BC@nZVI transport

Figure 5(b) shows the effects of porous media on B-BC@nZVI transport at a fixed flow velocity (0.11 mL/s). The steady-state relative C/C_0 ratios of B-BC@nZVI in the 10–20 and 30–40 mesh silica sands were 0.82 and 0.74, respectively. Although the differences in the C/C_0 ratios of the particles between the two sizes of silica sand investigated herein were small, it can still be concluded that the transport capacity of B-BC@nZVI increases as the size of the silica sand particles constituting the porous media increases. This effect can be ascribed to an increase in the surface area of the sand after deposition of BC@nZVI particles for the case of smaller silica particles, combined with the effects of strain, as observed in previous studies (Chrysikopoulos and Syngouna, 2014; Li and Ghoshal, 2016). Moreover, the elution concentrations of B-BC@nZVI in the silica sand column increased more sharply than those in soil and subsequently reached a steady-state at 4 PV, while in soil, steady-state was reached after 3 PV. Furthermore, the maximum C/C_0 value of BC@nZVI in the 30 mesh soil column was only 0.25, which was 57% lower than the value obtained in a similar-sized silica sand column (30–40 mesh silica sand). However, according to Fig. 5(b), the breakthrough curve of BC@nZVI showed a larger transport efficiency in soil than that of bare-nZVI. Additionally, the maximum C/C_0 value of B-BC@nZVI in the 30 mesh soil column was similar to the maximum C/C_0 value of C-BC@nZVI in the 30–40 mesh silica sand column (Figs. 2(b) and 5(a)), indicating better B-BC@nZVI transport.

3.3.3 Column transport of various BC@nZVI composites

As indicated in Fig. 6(a), the maximum relative concentration (C/C_0) of nZVI was only approximately 0.02 within 8 PV following injection, and at the end of the column, most of the nZVI was left. By contrast, the BC@nZVI composites distinctly improved the transport of nZVI in the silica sand column, and the maximum C/C_0 value was at least 25% higher than that of nZVI. The breakthrough curves of all of the BC@nZVI composites rose sharply in the first 2 PV and then slowly increased to a near steady-state plateau at 4 PV. The levels of the plateau (of C/C_0) differed among the four BC@nZVI composites, and the plateau of B-BC@nZVI was the highest. Additionally, the breakthrough curves of all of the BC@nZVI composites showed a slow but continuously increasing trend between 4 PV and 7 PV. Furthermore, B-BC@nZVI had the highest effluent concentration (C/C_0 = 0.74), followed by R-BC@nZVI (C/C_0 = 0.55), W-BC@nZVI (C/C_0 = 0.37) and C-BC@nZVI (C/C_0 = 0.26). These results indicated that B-BC was the most effective support in terms of improving the mobility of nZVI among the four prepared BCs, which is consistent with the sedimentation results.

Figure 6(b) presents the spatial distribution of the particles in the silica sand after the column was injected with 15 PV of particle suspension. The data in Fig. 6(b) are consistent with the breakthrough curves. Except for B-BC@nZVI, the RPs of all of the other particles typically exhibited a higher retention in the section adjacent to the column inlet and a rapid decrease in retention with increasing depth, especially for nZVI (retention decreased by nearly 63.5% as the depth increased from 2 cm to 4 cm). For B-BC@nZVI, the total residual particle content in the

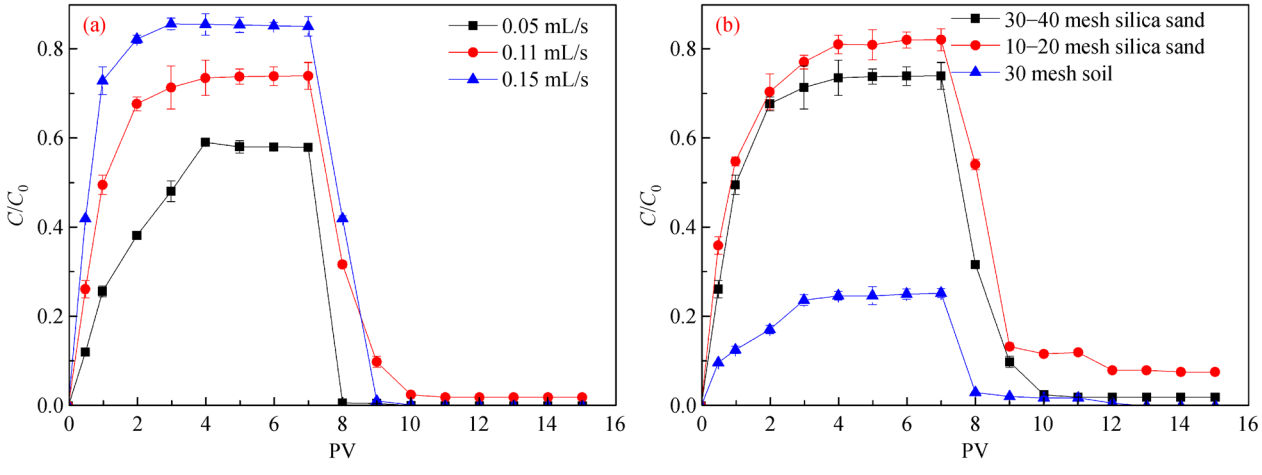

Fig. 5 Breakthrough curves of B-BC@nZVI at (a) different flow velocities in 30–40 mesh silica sand and (b) through three model porous media at 0.11 mL/s.

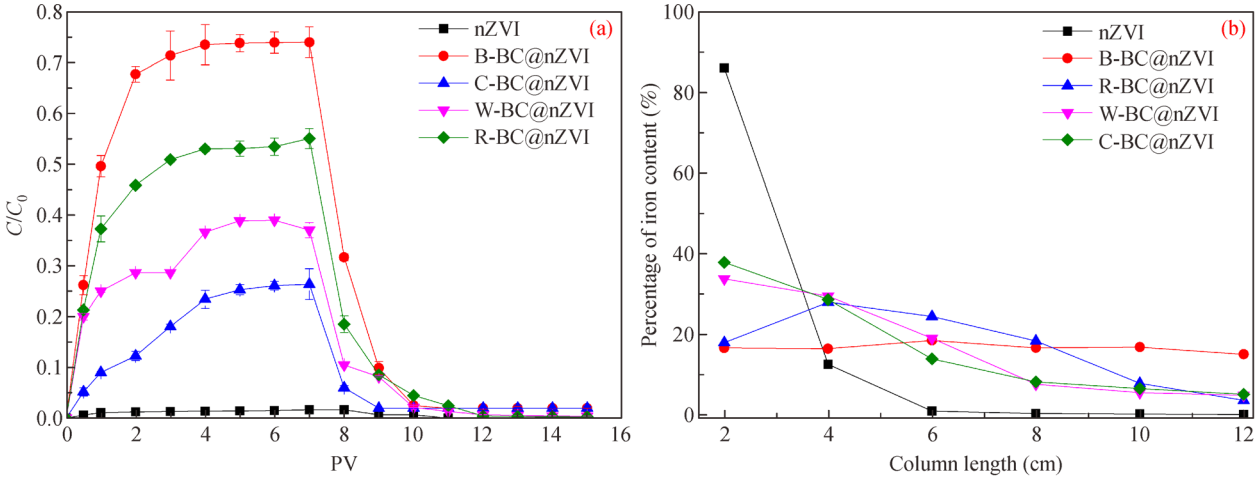

Fig. 6 Breakthrough curves of different particles in silica sand (a) and retention profiles of particles along the column length with 15 PV of particle suspension (b). (BC:nZVI = 1:1; particle concentration = 1 g/L; v = 0.11 mL/s; media size = 30–40 mesh silica sand).

column was the lowest, and the normalized content (M: M_{total}) remained steady at ~17% in all sections of the column. This result indicated that the residual particles were uniformly distributed in the column and the transport capability was the highest. These results suggest that the B-BC@nZVI composite has good stability and fluidity, which makes it a better material than the other materials tested herein for the in situ remediation.

As illustrated by the transport breakthrough curves and the RPs, the mobility values of the four types of BC@nZVI composites decreased in the following order: B-BC@nZVI > R-BC@nZVI > W-BC@nZVI > C-BC@nZVI, and this decrease was primarily related to differences in the BET SSAs of the four BCs (Table S2): the larger the SSA of a BC is, the more conducive the BC is to the dispersion of nZVI, which is more beneficial for the transport of nZVI. Moreover, the hydrodynamic diameter is considered a relevant property that is directly related to diffusivity and enhances particle mobility. In this paper, the hydrodynamic diameters of the particles as measured using the dynamic light scattering technique were 0.318 μm, 0.354 μm, 0.424 μm and 0.448 μm for B-BC@nZVI, R-BC@nZVI, W-BC@nZVI and C-BC@nZVI, respectively. Thus, enhanced mobility was observed for the composites with smaller particle sizes, which is consistent with previous research findings (Raychoudhury et al., 2010). Additionally, a more negative ζ-potential of the BCs was found to be beneficial for the mobility of the composites because the combination of BC and nZVI reduces the magnetic attraction and, consequently, enhances the overall repulsive interaction between the particles. Therefore, the impact of BC on nZVI mobility may be attributable to a combination of the abovementioned factors, but more detailed work is needed to ascertain the exact relationship between them.

3.4 BDE209 reactions with different particles under optimum conditions

The effects of different BC:nZVI mass ratios on BDE209 removal by BC@nZVI are illustrated in Fig. 7. Notably, the removal efficiency of BDE209 by BC@nZVI increased as the BC:nZVI mass ratios of the composites increased from 0.11:1 to 1:1. A removal efficiency of 66.8% was achieved with B-BC@nZVI (1:1) after 72 h, which was 30.1%, 23.3% and 17.4% higher than the removal efficiencies of B-BC@nZVI composites with mass ratios of 0.11:1, 0.25:1 and 0.5:1 (using the same amount of nZVI), respectively. This result may be ascribed to the fact that nZVI loading in BC significantly improves the dispersion, stability and mobility of the composite

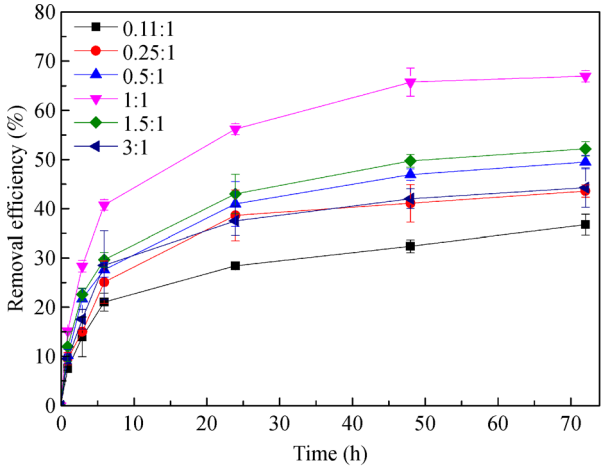

Fig. 7 Effect of BC:nZVI mass ratio on BDE209 removal by B-BC@nZVI (temperature, 25°C±2°C; dosage, 0.03 g/g; soil moisture content, 50%).

particles, which is conducive to improving the activity of the composite particles. The other reason may be an increase in the number of interaction sites between the composite nanoparticles and BDE209, in turn leading to increased removal rates. However, when the BC:nZVI mass ratio was increased from 1:1 to 3:1, the BDE209 removal efficiency decreased from 66.8% to 44.2%. A similar phenomenon was reported by other researchers (Dong et al., 2017; Yi et al., 2017). We deduced that the excess BC might have wrapped the nZVI particles or cut the active sites off the nZVI surfaces, thus inhibiting contact between BDE209 and nZVI, which reduced the BDE209 removal efficiency. Thus, the BC:nZVI mass ratio of 1:1 was found to be optimum and was selected for the synthesis of BC@nZVI particles, in accordance with the results of the stability tests and the column experiments described earlier in this paper.

The reactions of BDE209 with nZVI, BC and the four types of composite materials were measured over time under the optimum operating conditions, as shown in Fig. 8(a). BC achieved a low BDE209 removal efficiency (17.5%) at 72 h. Moreover, no Br^- ions was detected during the experiment with BC@nZVI. This finding implied that BDE209 removal from soil by BC occurred through adsorption without further debromination. By contrast, B-BC@nZVI, R-BC@nZVI, W-BC@nZVI and C-BC@nZVI achieved removal efficiencies of 66.8%, 52.3%, 45.8% and 37.5%, respectively, within a 72-h reaction time. The BDE209 removal efficiencies of the four BC@nZVI composites were higher than that of pure nZVI (35.4% within 72 h), demonstrating that the addition of BC helped improve the BDE209 removal performance of nZVI. The large SSA was a crucial factor in the composites achieving higher BDE209 removal efficiencies because BDE209 can be enriched by adsorption, thus increasing contact opportunities between nZVI and the target pollutant. Moreover, the loading of nZVI particles onto the surface or into the porous structure of BC reduced their agglomeration and improved their dispersibility, stability and mobility, which was conducive to enhancing the reactivity of the nZVI nanoparticles. Moreover, the composites provide more active sites for pollutant removal than pure nZVI does (Zhu et al., 2009; Petala et al., 2013; Dong et al., 2017). In addition, BC can act as an electron carrier (Kappler et al., 2014; Dong et al., 2017) due to its quinone content and aromatic structure, which increases the relative rate of electron transfer to the target pollutant, thus further accelerating the degradation of BDE209 by the nanoparticles. The differences among the four BC@nZVI composites can be explained as follows. The more stable and transportable the composites are, the higher their reactivity and removal efficiency; thus, BDE209 was removed at a faster rate by the B-BC@nZVI composites. In addition, the highest S content in B-BC (Table S2) may have also contributed to the highest removal efficiency of the B-BC@nZVI composites; this is consistent with multiple studies that have demonstrated that the reactivity of nZVI toward halogenated contaminants increases in the presence of sulfur compounds (Rajajayavel and Ghoshal, 2015; Fan et al., 2016). The presence of sulfur in BC may have contributed to the formation of either sulphide-modified nZVI or iron sulphide (FeS), which facilitates more efficient electron transfer due to the lower band gap of Fe_xS_y than Fe_xO_y (Turcio-Ortega et al., 2012) and the adsorption of more atomic hydrogen on the surface to favor the reductive degradation of organic pollutants (Han and Yan, 2016). Furthermore, sulphide modification of nZVI enhances the affinity between the hydrophobic surface of the particles and target hydrophobic groups (Cao et al., 2017).

We measured the Br^- ion content to determine whether BDE209 was actually degraded. The results in Fig. 8(b) indicate that the degree of formation of Br^- ions was the same as the removal efficiency; that is, the rate of

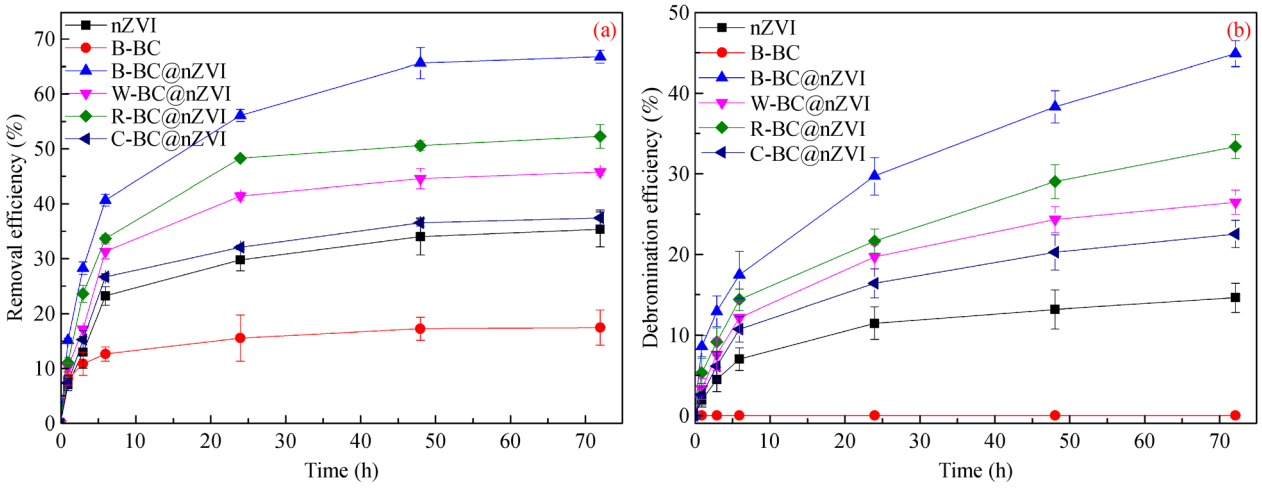

Fig. 8 (a) Removal efficiency of BDE-209 and (b) debromination efficiency of BDE-209 (BC:nZVI = 1:1; temperature = 25°C±2°C; dosage = 0.03 g/g; soil moisture content = 50%).

bromination increased rapidly in the first 24 h, followed by a slow increase of only 15.1% between 24 and 72 h of B-BC@nZVI treatment. The debromination rate induced by B-BC@nZVI was 30.2%, 22.3%, 18.3% and 11.5% higher than the rates induced by nZVI, C-BC@nZVI, W-BC@nZVI and R-BC@nZVI, respectively. These results further confirmed that B-BC@nZVI was the most reactive. Furthermore, BDE209 degradation was well described by pseudo-first-order kinetics (The specific formula is as follows Eqs. (2) and (3)) in Appendix A4. The results of the kinetic analysis also demonstrated that B-BC@nZVI was more effective in removing BDE209 than were C-BC@nZVI, W-BC@nZVI, R-BC@nZVI and nZVI (see Appendix A4, Table S3 and Fig. S3 for details). In summary, the loading of nZVI particles onto BC greatly improved their reactivity, and B-BC@nZVI was the most favorable for the removal of BDE209 from soil.

Based on the above discussion, we can conclude that the removal of BDE209 using nZVI loaded on BC involves reduction, debromination and adsorption. However, because of the observed low removal efficiency of neat BC for BDE209, the removal mechanism of BC@nZVI can be considered to depend mostly on the reductive properties of the nZVI particles. BC acts as a carrier that improves the distribution of nZVI, an adsorbent that enriches BDE209 in the composites and an electron transfer medium that promotes the reaction between nZVI and BDE209.

4 Conclusions

In this study, BC-supported nZVI particles were synthesized, and the feasibility of supporting nZVI on various BCs to enhance its stability, mobility and reactivity was investigated. It was found that the stability of BC@nZVI composites increased in proportion to the C/H ratio of the BC, while the mobility increased as the hydrodynamic diameter of the particles decreased and the BET SSA and negative ζ-potential of the BC increased. Moreover, the stability, mobility and reactivity of the composites peaked when the BC:nZVI mass ratio was 1:1; a lower mass of BC could not prevent the aggregation of nZVI particles, whereas excessive BC led to an increase in particle size and blocked the active sites of nZVI. The results of soil tests and column experiments indicated that B-BC@nZVI performed better than the composites and bare-nZVI. Additionally, the mobility of BC@nZVI increased with increasing flow velocity and increasing size of the solid phase in the porous media. The removal efficiency of BDE209 by B-BC@nZVI was the highest (66.8%). Removal was essentially considered to occur through an interaction between reductive removal and adsorption. The porous structure of BC adsorbed nZVI and enriched BDE209, thus diminishing the role of nZVI and reducing the bromination of BDE209. In summary, all of the results indicated that the use of BC as a support is effective for stabilizing nZVI and enhancing its transport and reactivity. The findings of this study can serve as a reference for the in situ remediation of pollutants by using BC-modified nZVI particles in the future.

Acknowledgements This work was supported by The National Key Research and Development Program of China (2018YFC1802802). This work was also supported by the Guangdong Technology Research Center for Ecological Management and Remediation of Water Systems (2014B090904077). Thanks to Eric Pokeung Tsang (Dept Sci & Environment Studies, Hong Kong Inst Educ, China).

Electronic Supplementary Material Supplementary material is available in the online version of this article at https://doi.org/10.1007/s11783-021-1388-4 and is accessible for authorized users.

References

Abbasi G, Li L, Breivik K (2019). Global historical stocks and emissions of PBDEs. Environmental Science & Technology, 53(11): 6330–6340

Ahmad M, Ahmad M, Usman A R A, Al-Faraj A S, Abduljabbar A S, Al-Wabel M I (2018). Biochar composites with nano zerovalent iron and eggshell powder for nitrate removal from aqueous solution with coexisting chloride ions. Environmental Science and Pollution Research International, 25(26): 25757–25771

Ahmad M, Lee S S, Dou X, Mohan D, Sung J K, Yang J E, Ok Y S (2012). Effects of pyrolysis temperature on soybean stover- and peanut shell-derived biochar properties and TCE adsorption in water. Bioresource Technology, 118: 536–544

Baumann T (2010). Nanoparticles in groundwater: Occurrence and applications. In: Frimmel F H, Niessner R, eds. Nanoparticles in the Water Cycle. Berlin: Springer Berlin Heidelberg, 23–34

Bolan N, Kunhikrishnan A, Thangarajan R, Kumpiene J, Park J, Makino T, Kirkham M B, Scheckel K (2014). Remediation of heavy metal (loid)s contaminated soils–to mobilize or to immobilize? Journal of Hazardous Materials, 266: 141–166

Cantrell K B, Hunt P G, Uchimiya M, Novak J M, Ro K S (2012). Impact of pyrolysis temperature and manure source on physicochemical characteristics of biochar. Bioresource Technology, 107: 419–428

Cao Z, Liu X, Xu J, Zhang J, Yang Y, Zhou J, Xu X, Lowry G V (2017). Removal of antibiotic florfenicol by sulfide-modified nanoscale zero-valent iron. Environmental Science & Technology, 51(19): 11269–11277

Cazetta A L, Pezoti O, Bedin K C, Silva T L, Paesano A J, Asefa T, Almeida V C (2016). Magnetic activated carbon derived from biomass waste by concurrent synthesis: efficient adsorbent for toxic dyes. ACS Sustainable Chemistry & Engineering, 4(3): 1058–1068

Chekli L, Brunetti G, Marzouk E R, Maoz-Shen A, Smith E, Naidu R, Shon H K, Lombi E, Donner E (2016). Evaluating the mobility of polymer-stabilised zero-valent iron nanoparticles and their potential to co-transport contaminants in intact soil cores. Environmental Pollution, 216: 636–645

Chintala R, Schumacher T E, Mcdonald L M, Clay D E, Malo D D, Papiernik S K, Clay S A, Julson J L (2014). Phosphorus sorption and

availability from biochars and soil/biochar mixtures. Clean-Soil, Air, Water, 42(5): 626–634

Chokwe T B, Magubane M N, Abafe O A, Okonkwo J O, Sibiya I V (2019). Levels, distributions, and ecological risk assessments of polybrominated diphenyl ethers and alternative flame retardants in river sediments from Vaal River, South Africa. Environmental Science and Pollution Research International, 26(7): 7156–7163

Chrysikopoulos C V, Syngouna V I (2014). Effect of gravity on colloid transport through water-saturated columns packed with glass beads: Modeling and experiments. Environmental Science & Technology, 48(12): 6805–6813

Cincinelli A, Martellini T, Misuri L, Lanciotti E, Sweetman A, Laschi S, Palchetti I (2012). PBDEs in Italian sewage sludge and environmental risk of using sewage sludge for land application. Environmental Pollution, 161: 229–234

Devi P, Saroha A K (2014). Synthesis of the magnetic biochar composites for use as an adsorbent for the removal of pentachlorophenol from the effluent. Bioresource Technology, 169: 525–531

Dong H, Deng J, Xie Y, Zhang C, Jiang Z, Cheng Y, Hou K, Zeng G (2017). Stabilization of nanoscale zero-valent iron (nZVI) with modified biochar for Cr(VI) removal from aqueous solution. Journal of Hazardous Materials, 332: 79–86

Eriksson P, Jakobsson E, Fredriksson A (2001). Brominated flame retardants: A novel class of developmental neurotoxicants in our environment? Environmental Health Perspectives, 109(9): 903–908

Fan D, O'brien Johnson G, Tratnyek P G, Johnson R L (2016). Sulfidation of nano zerovalent iron (nZVI) for improved selectivity during in-situ chemical reduction (ISCR). Environmental Science & Technology, 50(17): 9558–9565

Fang Z, Qiu X, Chen J, Qiu X (2011). Debromination of polybrominated diphenyl ethers by Ni/Fe bimetallic nanoparticles: influencing factors, kinetics, and mechanism. Journal of Hazardous Materials, 185(2–3): 958–969

Han Y, Yan W (2016). Reductive dechlorination of trichloroethene by zero-valent iron nanoparticles: reactivity enhancement through sulfidation treatment. Environmental Science & Technology, 50 (23): 12992–13001

He F, Zhao D, Liu J, Roberts C B (2007). Stabilization of Fe-Pd nanoparticles with sodium carboxymethyl cellulose for enhanced transport and dechlorination of trichloroethylene in soil and groundwater. Industrial & Engineering Chemistry Research, 46(1): 29–34

He F, Zhao D, Paul C (2010). Field assessment of carboxymethyl cellulose stabilized iron nanoparticles for in situ destruction of chlorinated solvents in source zones. Water Research, 44(7): 2360–2370

He F, Zhao D Y (2005). Preparation and characterization of a new class of starch-stabilized bimetallic nanoparticles for degradation of chlorinated hydrocarbons in water. Environmental Science & Technology, 39(9): 3314–3320

Hites R A (2004). Polybrominated diphenyl ethers in the environment and in people: A meta-analysis of concentrations. Environmental Science & Technology, 38(4): 945–956

Kanel S R, Goswami R R, Clement T P, Barnett M O, Zhao D (2008). Two dimensional transport characteristics of surface stabilized zero-valent iron nanoparticles in porous media. Environmental Science & Technology, 42(3): 896–900

Kappler A, Wuestner M L, Ruecker A, Harter J, Halama M, Behrens S (2014). Biochar as an electron shuttle between bacteria and Fe(III) minerals. Environmental Science & Technology Letters, 1(8): 339–344

Keiluweit M, Nico P S, Johnson M G, Kleber M (2010). Dynamic molecular structure of plant biomass-derived black carbon (biochar). Environmental Science & Technology, 44(4): 1247–1253

Keum Y S, Li Q X (2005). Reductive debromination of polybrominated diphenyl ethers by zerovalent iron. Environmental Science & Technology, 39(7): 2280–2286

La Guardia M J, Hale R C, Harvey E (2006). Detailed polybrominated diphenyl ether (PBDE) congener composition of the widely used penta-, octa-, and deca-PBDE technical flame-retardant mixtures. Environmental Science & Technology, 40(20): 6247–6254

Li J, Ghoshal S (2016). Comparison of the transport of the aggregates of nanoscale zerovalent iron under vertical and horizontal flow. Chemosphere, 144: 1398–1407

Liang B, Xie Y, Fang Z, Tsang E P (2014). Assessment of the transport of polyvinylpyrrolidone-stabilised zero-valent iron nanoparticles in a silica sand medium. Journal of Nanoparticle Research, 16(7): 2485–2496

Liu Z, Zhang F S, Wu J (2010). Characterization and application of chars produced from pinewood pyrolysis and hydrothermal treatment. Fuel, 89(2): 510–514

Lowry G V, Johnson K M (2004). Congener-specific dechlorination of dissolved PCBs by microscale and nanoscale zerovalent iron in a water/methanol solution. Environmental Science & Technology, 38 (19): 5208–5216

Meerts I, Letcher R J, Hoving S, Marsh G, Bergman A, Lemmen J G, Van Der Burg B, Brouwer A (2001). In vitro estrogenicity of polybrominated diphenyl ethers, hydroxylated PBDEs, and polybrominated bisphenol A compounds. Environmental Health Perspectives, 109(4): 399–407

Mohamed B A, Ellis N, Kim C S, Bi X (2017). The role of tailored biochar in increasing plant growth, and reducing bioavailability, phytotoxicity, and uptake of heavy metals in contaminated soil. Environmental Pollution, 230: 329–338

Petala E, Dimos K, Douvalis A, Bakas T, Tucek J, Zboril R, Karakassides M A (2013). Nanoscale zero-valent iron supported on mesoporous silica: characterization and reactivity for Cr(VI) removal from aqueous solution. Journal of Hazardous Materials, 261: 295–306

Quinn J, Geiger C, Clausen C, Brooks K, Coon C, O'hara S, Krug T, Major D, Yoon W S, Gavaskar A, Holdsworth T (2005). Field demonstration of DNAPL dehalogenation using emulsified zero-valent iron. Environmental Science & Technology, 39(5): 1309–1318

Rajajayavel S R, Ghoshal S (2015). Enhanced reductive dechlorination of trichloroethylene by sulfidated nanoscale zerovalent iron. Water Research, 78: 144–153

Raychoudhury T, Naja G, Ghoshal S (2010). Assessment of transport of two polyelectrolyte-stabilized zero-valent iron nanoparticles in porous media. Journal of Contaminant Hydrology, 118(3–4): 143–151

Shih Y H, Tai Y T (2010). Reaction of decabrominated diphenyl ether by zerovalent iron nanoparticles. Chemosphere, 78(10): 1200–1206

Su H, Fang Z, Tsang P E, Zheng L, Cheng W, Fang J, Zhao D (2016).

Remediation of hexavalent chromium contaminated soil by biochar-supported zero-valent iron nanoparticles. Journal of Hazardous Materials, 318: 533–540

Tiraferri A, Chen K L, Sethi R, Elimelech M (2008). Reduced aggregation and sedimentation of zero-valent iron nanoparticles in the presence of guar gum. Journal of Colloid and Interface Science, 324(1–2): 71–79

Turcio-Ortega D, Fan D, Tratnyek P G, Kim E J, Chang Y S (2012). Reactivity of Fe/FeS nanoparticles: electrolyte composition effects on corrosion electrochemistry. Environmental Science & Technology, 46(22): 12484–12492

Wang D, Zhang W, Hao X, Zhou D (2013a). Transport of biochar particles in saturated granular media: Effects of pyrolysis temperature and particle size. Environmental Science & Technology, 47(2): 821–828

Wang Y, Zhong B, Shafi M, Ma J, Guo J, Wu J, Ye Z, Liu D, Jin H (2019). Effects of biochar on growth, and heavy metals accumulation of moso bamboo (*Phyllostachy pubescens*), soil physical properties, and heavy metals solubility in soil. Chemosphere, 219: 510–516

Wang Z, Zheng H, Luo Y, Deng X, Herbert S, Xing B (2013b). Characterization and influence of biochars on nitrous oxide emission from agricultural soil. Environmental Pollution, 174: 289–296

Wu J, Yi Y, Li Y, Fang Z, Tsang E P (2016). Excellently reactive Ni/Fe bimetallic catalyst supported by biochar for the remediation of decabromodiphenyl contaminated soil: Reactivity, mechanism, pathways and reducing secondary risks. Journal of Hazardous Materials, 320: 341–349

Wu W, Yang M, Feng Q, Mcgrouther K, Wang H, Lu H, Chen Y (2012). Chemical characterization of rice straw-derived biochar for soil amendment. Biomass and Bioenergy, 47: 268–276

Xie Y, Fang Z, Cheng W, Tsang P E, Zhao D (2014). Remediation of polybrominated diphenyl ethers in soil using Ni/Fe bimetallic nanoparticles: Influencing factors, kinetics and mechanism. Science of the Total Environment, 485– 486: 363–370

Xu J, Gao N, Tang Y, Deng Y, Sui M (2010). Perchlorate removal using granular activated carbon supported iron compounds: Synthesis, characterization and reactivity. Journal of Environmental Sciences-China, 22(11): 1807–1813

Yan J, Han L, Gao W, Xue S, Chen M (2015). Biochar supported nanoscale zerovalent iron composite used as persulfate activator for removing trichloroethylene. Bioresource Technology, 175: 269–274

Yi Y, Tu G, Zhao D, Tsang P E, Fang Z (2019). Pyrolysis of different biomass pre-impregnated with steel pickling waste liquor to prepare magnetic biochars and their use for the degradation of metronidazole. Bioresource Technology, 289: 12163–12169

Yi Y, Wu J, Wei Y, Fang Z, Tsang E P (2017). The key role of biochar in the rapid removal of decabromodiphenyl ether from aqueous solution by biochar-supported Ni/Fe bimetallic nanoparticles. Journal of Nanoparticle Research, 19(7): 245–260

Zhang M, He F, Zhao D, Hao X (2017). Transport of stabilized iron nanoparticles in porous media: Effects of surface and solution chemistry and role of adsorption. Journal of Hazardous Materials, 322: 284–291

Zhang W, Liu K, Li J, Liang J, Lin K (2015). Impacts of BDE209 addition on Pb uptake, subcellular partitioning and gene toxicity in earthworm (*Eisenia fetida*). Journal of Hazardous Materials, 300: 737–744

Zhou Y, Gao B, Zimmerman A R, Chen H, Zhang M, Cao X (2014). Biochar-supported zerovalent iron for removal of various contaminants from aqueous solutions. Bioresource Technology, 152: 538–542

Zhu H, Jia Y, Wu X, Wang H (2009). Removal of arsenic from water by supported nano zero-valent iron on activated carbon. Journal of Hazardous Materials, 172(2–3): 1591–1596

Zhuang Y, Ahn S, Seyfferth A L, Masue-Slowey Y, Fendorf S, Luthy R G (2011). Dehalogenation of polybrominated diphenyl ethers and polychlorinated biphenyl by bimetallic, impregnated, and nanoscale zerovalent iron. Environmental Science & Technology, 45(11): 4896–4903